RSC Advances

PAPER

View Article Online
View Journal | View Issue

Cite this: *RSC Adv.*, 2023, **13**, 5273

Regulation and photocatalytic degradation mechanism of a hydroxyl modified UiO-66 type metal organic framework

Shixiong Li, *[ab] Shaolong Yang,[ab] Guichun Liang,[a] Mulun Yan,[a] Chengting Wei[a] and Yan Lu[a]

Received 1st January 2023
Accepted 6th February 2023

DOI: 10.1039/d3ra00004d

rsc.li/rsc-advances

Photocatalytic performance can be effectively improved by modifying the functional groups on the organic ligands of metal organic frameworks (MOFs). Herein, the hydroxyl-modified UiO-66 type MOF: UIO-66-2OH(2,3), was successfully synthesized by the method of ligand exchange by the 2,3-dihydroxyterephthalic acid and UIO-66 as raw materials. The mechanism of photocatalytic degradation of methylene blue (MB) by UIO-66-2OH(2,3) shows that the hydroxyl functional group on the organic ligand regulates its electronegativity and expands its light absorption range. The decomposition of MB is carried out in multiple steps under the oxidation of the hydroxyl radical (˙OH). This research result shows the direction for guiding the synthesis of efficient photocatalysts and clarifying the light absorption of MOFs regulated by hydroxyl functional groups.

1. Introduction

Photocatalytic oxidation technology can effectively solve the problems of environmental pollution and energy shortage facing the world today.[1–7] Design and synthesis of photocatalysts with high efficiency of light utilization and acid and alkali resistance are the prerequisites for the application of this technology. Since Fujishima reported in 1972 that TiO_2 inorganic semiconductor electrodes irradiated by light can decompose water to prepare H_2, the photocatalytic technology has received extensive attention in recent years.[8–11] Although TiO_2 is considered to be an inorganic semiconductor material with good photocatalytic reaction activity, semiconductor TiO_2 has a large forbidden bandwidth (E_g = 3.0–3.2 eV), and only about 4% of the ultraviolet light in sunlight can meet this energy. Therefore, scientists have used a variety of modification methods to improve the photocatalytic activity of TiO_2, such as changing its morphology,[12] doping and loading it.[13,14] At the same time, many inorganic semiconductor materials with good photocatalytic properties have also been discovered. They are include ZnO,[15] CdS,[16] Fe_2O_3,[17] and BiOX (X = Cl, Br, I).[18]

Metal–Organic Frameworks (MOFs) are a type of coordination polymer with an open framework and potential voids.[19] They not only have super-high specific surface area, abundant sites, and the structure is easy to modify. They have been extensively studied in gas adsorption storage and separation,[20] organic pollutants adsorption,[21] photocatalytic degradation,[22–24] and biological drug delivery.[25] Compared with traditional semiconductors, MOFs have more advantages as photocatalysts because of their adjustable organic ligands and metal ions. However, the photocatalytic efficiency of most current MOFs is generally low. In response to this, the scientists have adopted a series of strategies to enhance the absorption of visible light by MOFs and improve the efficiency of charge separation. One of the effective and simple methods is to modify the functional groups on the organic ligands. For example, the UIO-66-NH_2,[26] and MIL-68(In)-NH_2,[27] which have visible light response, are through the introduction of –NH_2 on the ligand. The authors' previous research[1] also found that the introduction of different electron-donating group into MIL-101(Fe)-X and UIO-66-X (X = –OH, –NH_2, –COOH, –NO_2, –H), among which the –OH modified MOFs have the best photocatalytic performance. And follow the rule of –OH > –NH_2> –COOH > –NO_2> –H. It can be predicted that there are more electron-donating groups in MOFs, and their photocatalytic performance should be better.

In this paper, the hydroxyl-modified MOF: UIO-66-2OH(2,3) was successfully synthesized by the method of ligand exchange by the 2,3-dihydroxyterephthalic acid and UIO-66 as raw materials, under the conditions of hydrothermal synthesis reaction. The structure of UIO-66-2OH(2,3) is characterized by Fourier infrared (IR), X-ray powder diffraction (XRD), and X-ray photoelectron spectroscopy (XPS). The effect of pH on the photocatalytic performance and the stability of the photocatalyst were explored. The results show that UIO-66-2OH(2,3) can rapidly degrade MB, and its performance is better than neutral under acidic conditions. The two uncoordinated hydroxyl groups (–OH) in the aromatic ring of UIO-66-2OH(2,3)

[a]*School of Mechanical and Resource Engineering, Wuzhou University, Wuzhou, Guangxi 543002, P. R. China. E-mail: lsx1324@163.com*
[b]*School of Chemistry and Chemical Engineering, Guangxi University, Nanning, 530004, P. R. China*

structure can effectively control its electronegativity and expand the absorption of light.

2. Experimental

2.1 Reagents and chemicals

All solvents and chemicals are commercial reagents and used without further purification. The terephthalic acid, 2,3-dihydroxyterephthalic acid, $ZrCl_4$, *N*,*N*-dimethylformamide, and methanol both were analytically pure, and purchased from Energy Chemical Co., Ltd. (Shanghai, China).

2.2 Instruments

The Nicolet 5DX FT-IR spectrometer was used to characterize and test the presence of hydroxyl functional groups in the UIO-66-2OH(2,3). The structure of UIO-66-2OH(2,3) was tested and analyzed by using Rigaku's D/max 2500 X-ray powder diffractometer (XRD). The test conditions were as follows: Cu Kα (λ = 0.156 04 nm), tube voltage was 40 kV, tube current was 150 mA, graphite monochromator, 2θ was 5° to 65°. The composition and valence state of the elements in the UIO-66-2OH(2,3) were determined by using the ESCALAB250 X-ray photoelectron spectroscopy (XPS) of Thermo Fisher Scientific with a base pressure of 1.33×10^{-7} Pa. The morphology of UIO-66-2OH(2,3) was observed by the Hitachi SU8010 scanning electron microscope (SEM), the acceleration voltage during the test was 1.0 kV. The light absorption behavior of UIO-66-2OH(2,3) was tested and analyzed by using UV-2700 from SHIMADZU of Japan, $BaSO_4$ as a reference. The specific surface area of UIO-66-2OH(2,3) was tested at 77 K by AUTO CHEM II2920 from American Micro Instrument Company. The zeta potential (mV) of UIO-66 and UIO-66-2OH(2,3) were measured by JS94H microelectrophoresis apparatus. The free radicals produced during the photocatalytic degradation of UIO-66-2OH(2,3) were determined by using an electronic paramagnetic resonance instrument (ADANl SPlNSCAN X, Germany). The visible light of photocatalytic reaction required in the experiment was carried out on a 1000 W xenon lamp catalytic reactor.

2.3 Synthesis of UIO-66

The UIO-66 was synthesized according to the method reported in the literature.[1] The experimental steps are as follows: a mixture of $ZrCl_4$ (3.495 g, 15 mmol) and terephthalic acid (2.491 g, 15 mmol) in 115 mL DMF was dissolved by ultrasonic wave. After the mixed solution was evenly dispersed, it was sealed in a 250 mL polytetrafluoroethylene (PTFE) reactor and heated in an oven at 120 °C for 24 h. After the reaction, it was cooled to room temperature, the solvent was removed by centrifugation, and the white solid powder obtained was collected. The white solid powder was collected and washed three times with DMF and methanol, and dried in a vacuum drying oven at 120 °C for 16 h. Finally, the UIO-66 white powder was obtained.

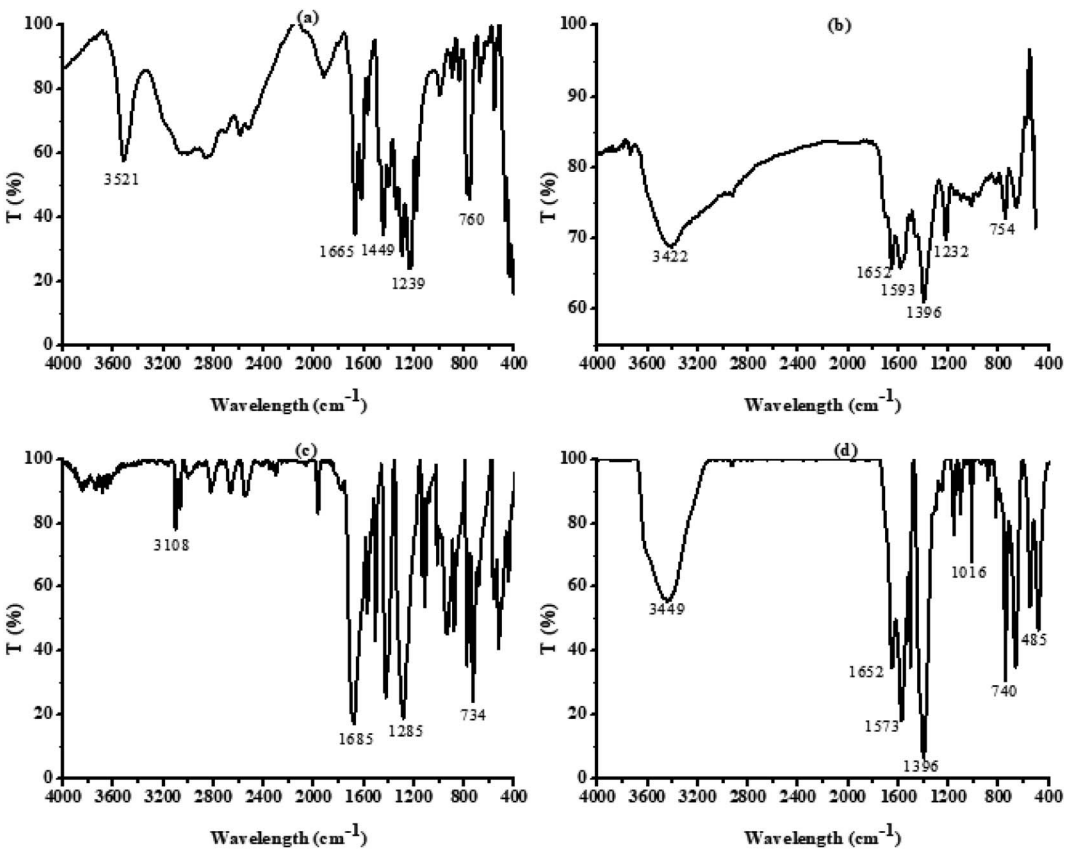

Fig. 1 IR of (a) 2,3-dihydroxyterephthalic acid, (b) UIO-66-2OH(2,3), (c) terephthalic acid, and (d) UIO-66.

2.4 Synthesis of UIO-66-2OH(2,3)

The UIO-66-2OH(2,3) was synthesized by the method of ligand exchange under the conditions of hydrothermal synthesis. The experimental steps are as follows: a mixture of UIO-66 (0.1000 g) and 2,3-dihydroxyterephthalic acid (0.1000 g) in 15 mL DMF, then it was sealed in a 23 mL polytetrafluoroethylene (PTFE) reactor and heated in an oven at 120 °C for 24 h. After the reaction, it was cooled to room temperature, and obtained yellow-brown precipitation. The precipitation was washed three times with 10 mL DMF and anhydrous methanol, and obtained pure UIO-66-2OH(2,3). Yield 98% (based on Zr^{4+}). IR data for UIO-66-2OH(2,3) (KBr, cm^{-1}): 3422 (m), 2922 (w), 1711 (w), 1652 (s), 1593 (s), 1466 (w), 1396 (s), 1232 (s), 1149 (w), 1108 (w), 1018 (w), 952 (w), 821 (w), 754 (m), 655 (m), and 558 (m). Elemental analyses *calc.* (%) for $[C_{48}H_{24}Zr_6O_{44}]$: C 31.10, H 1.30. Found: C 31.08, H 1.31.

2.5 Photocatalysis experiment

The photocatalytic properties of UIO-66-2OH(2,3) were studied by using the MB as organic pollutants. The specific process of the photocatalysis experiment was as follows: the dosage of photocatalyst was 0.0100 g; the initial concentration of MB was $c_0 = 10$ mg L^{-1}, and the dosage was 50 mL; the pH value during the photocatalysis experiment was 1, 3, 5, 7 and was measured with a Mettler pH meter; the photocatalytic reaction was carried out using an 800 W xenon lamp (A UV filter was added to the source to ensure removal the light of below 420 nm before the start of the photocatalytic reaction. At this time, the light irradiation intensity measured by the photometer was about 15 W m^{-2}). After the photocatalytic reaction was carried out for a certain period of time, the absorbance of MB in the solution was measured at 664 nm using an ultraviolet-visible spectrophotometer. The corresponding concentration of MB was calculated by the standard curve $A = 0.0708c + 0.0008$ ($R^2 = 0.9998$), where A is the abbreviation of absorbance and the c is the abbreviation of concentration. The photocatalytic degradation performance was evaluated by the change of MB concentration before and after the reaction. The degradation rate was calculated as follows:

$$R = \left(1 - \frac{c_t}{c_0}\right) \times 100\%$$

where R is the degradation rate (%).

3. Results and discussion

3.1 Structure of UIO-66-2OH(2,3)

The hydroxyl-modified MOF: UIO-66-2OH(2,3) was successfully synthesized by the method of ligand exchange by the 2,3-dihydroxyterephthalic acid and UIO-66 as raw materials, under the conditions of hydrothermal synthesis reaction. The hydrothermal synthesis gives a unique combination of pressure and temperature conditions for crystallization of MOFs and derived composites.[28–30] The structure of UIO-66-2OH(2,3) is characterized by IR, XRD, and XPS. The results show that its chemical

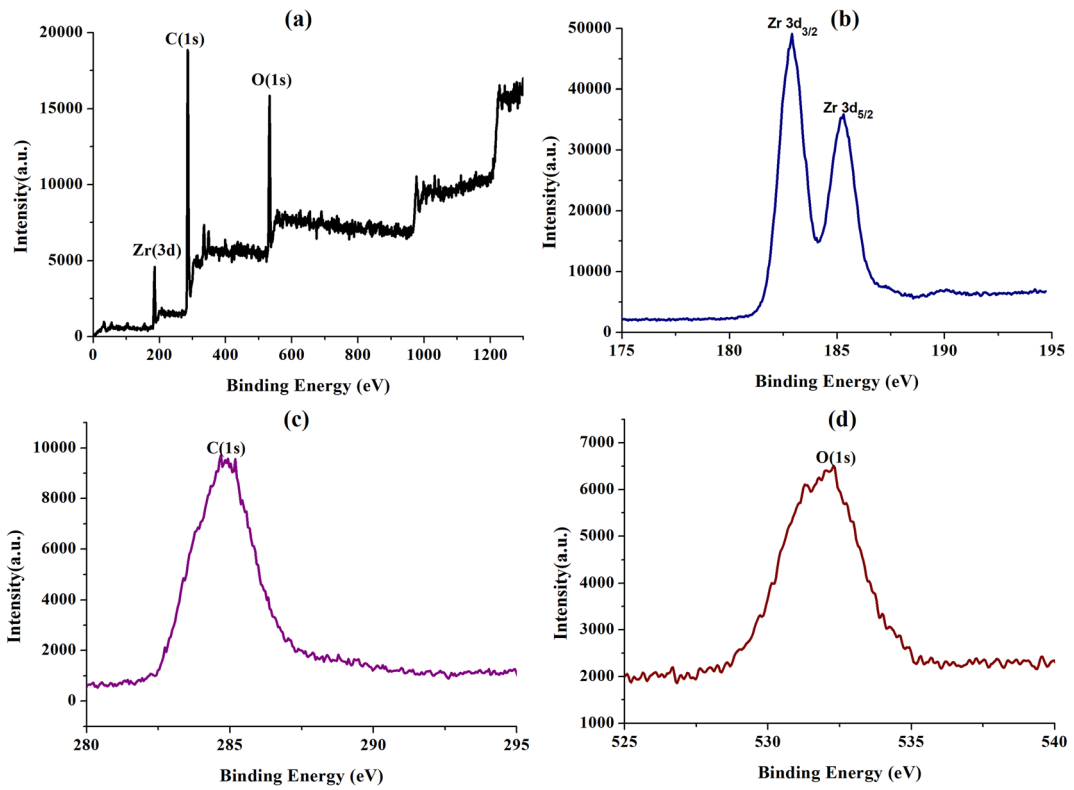

Fig. 2 XPS of UIO-66-2OH(2,3). (a) Survey; (b) Zr(3d); (c) C(1s); (d) O(1s).

formula is $C_{48}H_{24}Zr_6O_{44}$, which has a similar structure to UIO-66.

3.1.1 IR. The IR characterization can analyzes the functional groups contained in the material. The IR of 2,3-dihydroxyterephthalic acid (Fig. 1a) shows that it has infrared absorption vibration peaks at 3521 cm^{-1}, 2869 cm^{-1}, 1920 cm^{-1}, 1665 cm^{-1}, 1615 cm^{-1}, 1568 cm^{-1}, 1490 cm^{-1}, 1449 cm^{-1}, 1406 cm^{-1}, 1353 cm^{-1}, 1305 cm^{-1}, 1239 cm^{-1}, 1180 cm^{-1}, 994 cm^{-1}, 899 cm^{-1}, 845 cm^{-1}, 760 cm^{-1}, 672 cm^{-1}, and 564 cm^{-1}. The peak at 3521 cm^{-1} can be attributed to the absorption peak of –OH. This is a characteristic functional group that terephthalic acid does not have (Fig. 1c). The peak at 1239 cm^{-1} can be attributed to the absorption peak of –CO. The peak at 2869 cm^{-1}, 1665 cm^{-1}, and 994 cm^{-1} can be attributed to the absorption peak of –COOH. When the 2,3-dihydroxyterephthalic acid reacted with Zr^{4+} to form the UIO-66-2OH(2,3), its infrared absorption peak changed significantly. The IR spectrum of UIO-66-2OH(2,3) (Fig. 1b) is similar to that of UIO-66 (Fig. 1d). The IR of UIO-66-2OH(2,3) shows that it has infrared absorption vibration peaks at 3422 cm^{-1}, 2922 cm^{-1}, 1711 cm^{-1}, 1652 cm^{-1}, 1593 cm^{-1}, 1466 cm^{-1}, 1396 cm^{-1}, 1232 cm^{-1}, 1149 cm^{-1}, 1108 cm^{-1}, 1018 cm^{-1}, 952 cm^{-1}, 821 cm^{-1}, 754 cm^{-1}, 655 cm^{-1}, and 558 cm^{-1}. The peak at 1652 cm^{-1} can be attributed to the –C=O of –COOH. This indicates that the hydroxyl group on the carboxyl group has lost –H, causing the carbonyl group to move to the low frequency region. The infrared test shows that the 2,3-dihydroxyterephthalic acid had reacted with Zr^{4+} to form a complex.

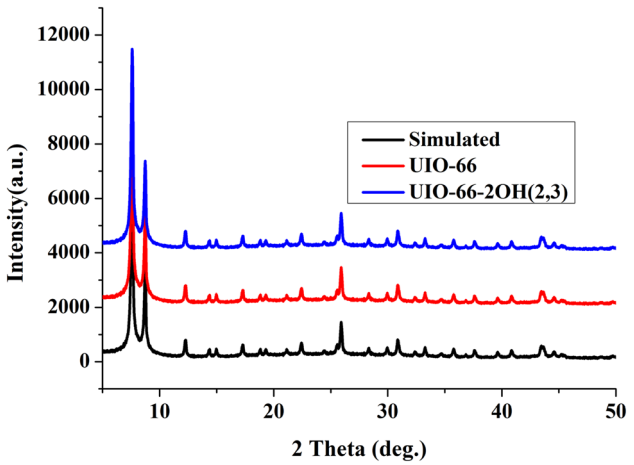

Fig. 3 XRD of UIO-66, and UIO-66-2OH(2,3).

3.1.2 XPS. The XPS can be used to analyze the element composition and valence of materials. The XPS of UIO-66-2OH(2,3) (Fig. 2a) shows that it is mainly composed of three elements: Zr, C, and O. The characteristic peak at 182.90 and 185.25 eV (Fig. 2b) are attributed to Zr $3d_{5/2}$ and Zr $3d_{3/2}$ orbitals of UIO-66-2OH(2,3). The characteristic peak at 284.66 eV (Fig. 2c) is attributed to C 1s orbitals of UIO-66-2OH(2,3). The characteristic peak at 532.22 eV (Fig. 2d) is attributed to O 1s orbitals of UIO-66-2OH(2,3). These elements are similar to the characteristic peaks of XPS reported in the literature.[1,24,31]

3.1.3 XRD. The XRD can be used to analyze the crystal structure of materials. The peaks at 7.62°, 8.77°, 12.29°, 14.34°, 14.99°, 17.21°, 18.85°, 19.26°, 21.23°, 22.45°, 24.50°, 25.89°, 28.27°, 29.92°, 30.89°, 32.46°, 33.27°, 34.67°, 35.81°, 36.88°, 37.62°, 39.67°, 40.82°, 43.44°, and 44.59° (Fig. 3) are consistent

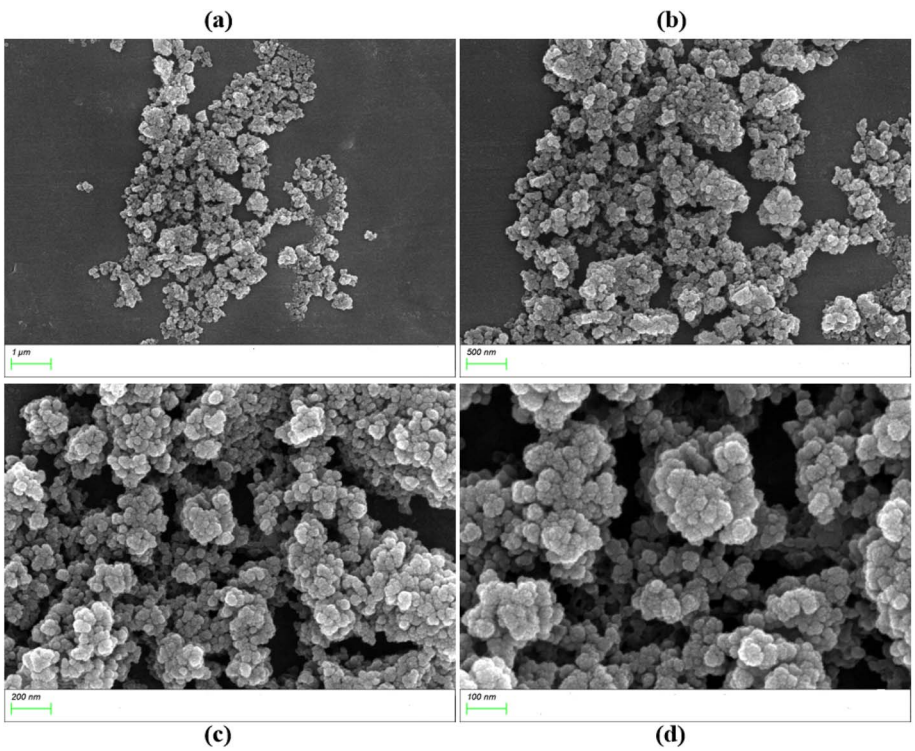

Fig. 4 SEM of UIO-66-2OH(2,3).

with the theoretical diffraction peaks of UIO-66. This shows that UIO-66, and UIO-66-2OH(2,3) have been successfully synthesized.

3.2 SEM

The size of the photocatalyst solid particles will affect their specific surface area and photocatalytic degradation performance. Generally, nano-level photocatalysts have good photocatalytic performance. The scanning electron microscopy (SEM) of UIO-66-2OH(2,3) (Fig. 4) shows that its morphology is quincunx with a particle size of about 50 nm.

3.3 N_2 adsorption–desorption isotherm

The specific surface area of photocatalysts will affect their ability to adsorb pollutants, thereby affecting the performance of photocatalytic degradation of organic pollutants. The N_2 adsorption–desorption isotherm can be used to measure the specific surface area, pore size and pore volume of the photocatalyst. The test results showed that the UIO-66-2OH(2,3), and UIO-66 are typical S-type adsorption curves (Fig. 5 and Table 1). It can be seen from the Fig. 5 that the surface area of UIO-66-2OH(2,3) is 570 $cm^2\ g^{-1}$. Since the UIO-66-2OH(2,3) has two –OH functional groups, its specific surface area is smaller than that reported in the literature of UIO-66. Its specific surface area is similar to UIO-66-NH_2 and UIO-66-NO_2.[1]

3.4 UV-Vis DRS

The ultraviolet-visible diffuse reflectance spectroscopy (UV-Vis DRS) can be used to judge the light absorption behavior of the photocatalyst, and the choice of light source in the photocatalysis process. The UIO-66-2OH(2,3) has strong light absorption in both the UV and visible regions when the $BaSO_4$ was used as a blank control experiment (Fig. 6). The UIO-66-2OH(2,3) absorbed more than 50% of light in the visible light range of 400–540 nm. But, the UIO-66 absorbed light less than 98% in the visible light range of 400–445 nm. So, the UIO-66-2OH(2,3) has stronger visible light absorption than UIO-66. Through the formula $E_g = 1240/\lambda_g$, the band gap (E_g) of UIO-66-2OH(2,3) can be calculated as 2.6 eV. So, the UIO-66-2OH(2,3) can perform photocatalytic degradation experiments under visible light conditions.

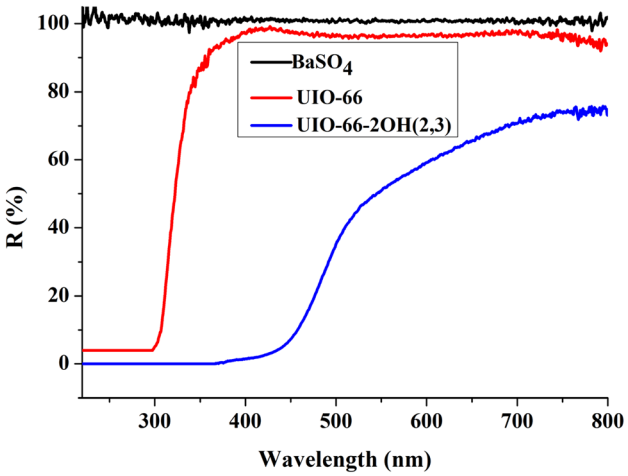

Fig. 6 UV-Vis DRS spectra of UIO-66, and UIO-66-2OH(2,3).

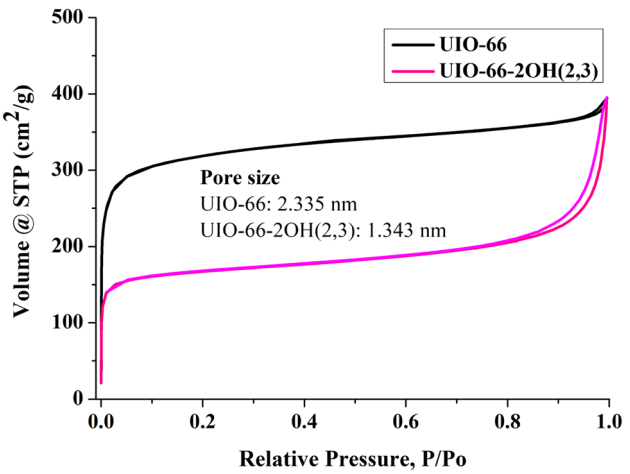

Fig. 5 N_2 adsorption–desorption isotherms for UIO-66-2OH(2,3), and UIO-66.

Table 1 Specific surface area, pore size, and pore volume of UIO-66-2OH(2,3)

Sample	Specific surface area ($cm^2\ g^{-1}$)	Pore size (nm)	Pore volume ($cm^3\ g^{-1}$)
UIO-66	1050	2.335	0.4467
UIO-66-2OH(2,3)	570	1.343	0.3012

3.5 Photocatalytic performance

The methylene blue (MB) is used as an organic pollutant[32–34] to explore the photocatalytic performance of UIO-66-2OH(2,3) under visible light irradiation. Since UIO-66-2OH(2,3) also has a larger specific surface area, it needs to be considered the experiment of its adsorption of MB. Therefore, the adsorption of UIO-66-2OH(2,3) and the photocatalytic degradation of MB experiments (Fig. 7) were carried out under the same conditions to illustrate its photocatalytic performance. A blank control experiment of adsorption (Fig. 7a) and photocatalytic degradation (Fig. 7b) was conducted without adding UIO-66-2OH(2,3).

From Fig. 7a, it is clear that UIO-66-2OH(2,3) can absorb a certain amount of MB at different pH. The adsorption equilibrium can be reached after 80 minutes of adsorption. Among them, at pH = 1, 3, 5, and 7, the removal rate of MB adsorbed by UIO-66-2OH(2,3) (Fig. 7a) is about 50.1%, 51.8%, 53.5%, and 52.3%, respectively. However, the UIO-66-2OH(2,3) can rapidly degrade MB in 100 minutes. Among them, at pH = 1, 3, 5, and 7, the removal rates of UIO-66-2OH(2,3) photocatalytic degradation of MB (Fig. 7b) are 100%, 99.6%, 99.2%, and 87.3%, respectively. By comparing the performance of UIO-66-2OH(2,3) photocatalytic degradation of MB under different pH conditions, it can be found that the performance of the photocatalyst under acidic conditions is better than that under neutral conditions. Among them, the photocatalytic performance is the

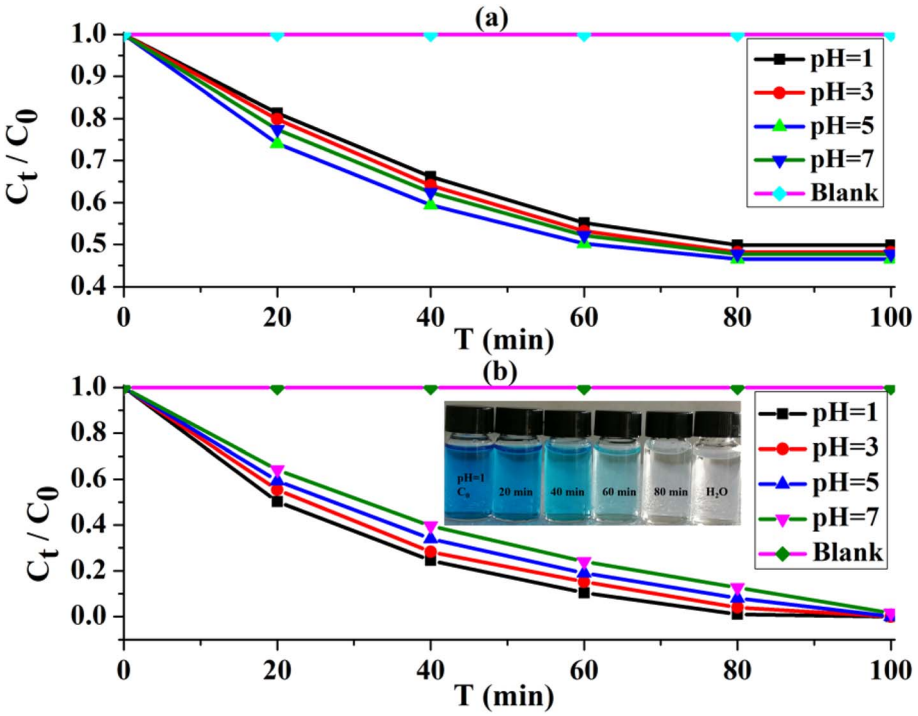

Fig. 7 The performance of removing MB by UIO-66-2OH(2,3): (a) adsorption; (b) photocatalytic degradation.

best at pH = 1, at this time its photocatalytic degradation rate of MB can reach 0.00625 mg min^{-1} L^{-1}. This performance is superior to that reported in the literature for the photocatalytic degradation of MB by UIO-66-2OH(2,5).[31] It can be seen that the performance of UIO-66-2OH(2,3) photocatalytic degradation of MB under acidic conditions is better than that of neutral conditions. This may be because when it is acidic, the UIO-66-2OH(2,3) surface adsorbs the H^+ and is positively charged.[1] The photo-generated electrons in the photocatalytic process are adsorbed to the surface, prolonging the time for it to combine with holes, thereby improving the photocatalytic performance. In addition, due to the isolated two hydroxyl functional groups on the structure of UIO-66-2OH(2,3), they can effectively increase the electronegativity of the photocatalyst, thereby effectively separating photogenerated electrons in photocatalytic degradation experiments. When UIO-66 and UIO-66-2OH(2,3) were suspended in different aqueous solutions with pH 1, 3, 5, and 7, their zeta potential (mV) was tested. The test results (Table 2) show that the zeta potential (mV) of UIO-66 and UIO-66-2OH(2,3) in acid is greater than that in neutral. And at the same pH, the zeta potential (mV) of UIO-66-2OH(2,3) is greater than UIO-66. The zeta potential (mV) of UIO-66 at pH 1, 3, 5, and 7 is 35.57, 20.69, 13.20, and 5.77, respectively. However, the UIO-66-2OH(2,3) has a very high zeta potential (Table 2) at pH 1, 3, 5, and 7, which are 46.47, 33.12, 26.32, and 19.56, respectively. This further proves that the performance of UIO-66-2OH(2,3) in acid is better than that in neutral.

Table 2 Zeta potential (mV) of UIO-66 and UIO-66-2OH(2,3) in water at pH 1, 3, 5, and 7

	Zeta potential (mV)	
pH sample	UIO-66	UIO-66-2OH(2,3)
1	35.57	46.47
3	20.69	33.12
5	13.20	26.32
7	5.77	19.56

3.6 Cyclic experiment

The UIO-66-2OH(2,3) was collected by centrifugation after its photocatalytic degradation of MB at pH = 1. The X-ray powder

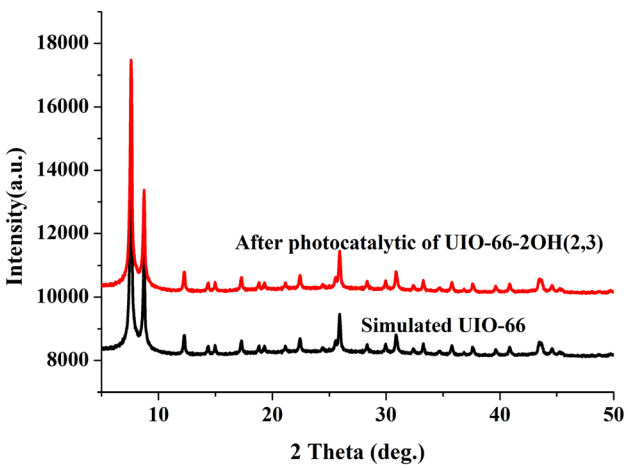

Fig. 8 XRD of UIO-66-2OH(2,3) after photocatalytic degradation of MB.

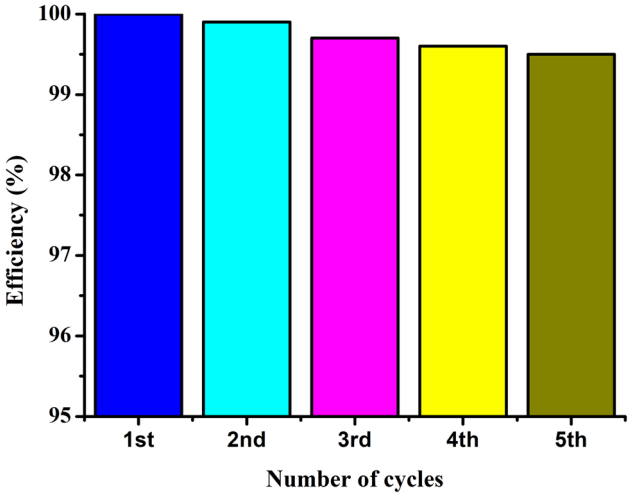

Fig. 9 Cyclic experiment.

diffraction was used to determine its structure. XRD (Fig. 8) shows that the structure after photocatalytic degradation of MB is the same as the original structure. It can be seen that UIO-66-2OH(2,3) has good stability. The efficiency of photocatalytic degradation of one cycle can still reach 100% (Fig. 9). The efficiency of photocatalytic degradation of five cycles can still reach 99.5%. It has the potential for practical application. The present work also contributes to the development of various dye pollutant degradation systems.[35,36]

3.7 Photocatalytic mechanism

The UV-Vis DRS spectrum (Fig. 6) of UIO-66 indicates that it is a white powder solid and can only absorb ultraviolet light. However, the UIO-66-2OH(2,3) is a light yellow solid and has ultraviolet and visible light absorption. It is a very interesting phenomenon that the absorption range of MOFs can be extended when two hydroxyl groups (-OH) are introduced into the terephthalic acid ligand. This may be due to the aromatic ring and –OH functional groups on 2,3-dihydroxyterephthalic acid ligand. The lone pair electrons on the –OH functional groups can be transferred to the aromatic ring in the form of p–π conjugation, thereby enhancing the electronegativity of the aromatic ring (Fig. 10). The increased electronegativity on the aromatic ring of the organic ligand can be transferred to Zr(IV) through the coordinated carboxyl oxygen atom. Therefore, the electronegativity of MOF can be enhanced by introducing uncoordinated –OH into the ligand, thus causing it to expand the absorption range of light.

The experiment of photocatalytic degradation of UIO-66-2OH(2,3) was carried out by adding DMPO to the solution with pH = 7 when the *tert*-butanol as the blank control experiment. The free radicals generated during the reaction were detected by electronic paramagnetic resonance (EPR). The EPR (Fig. 11) in the process of UIO-66-2OH(2,3) photocatalytic

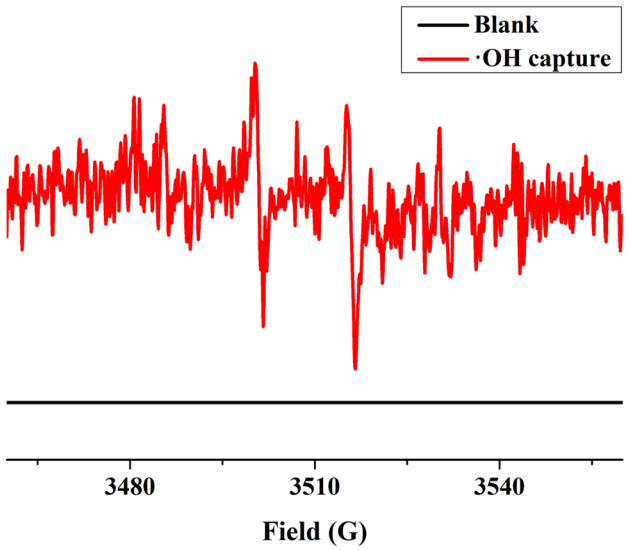

Fig. 11 Determination of the free radicals by EPR.

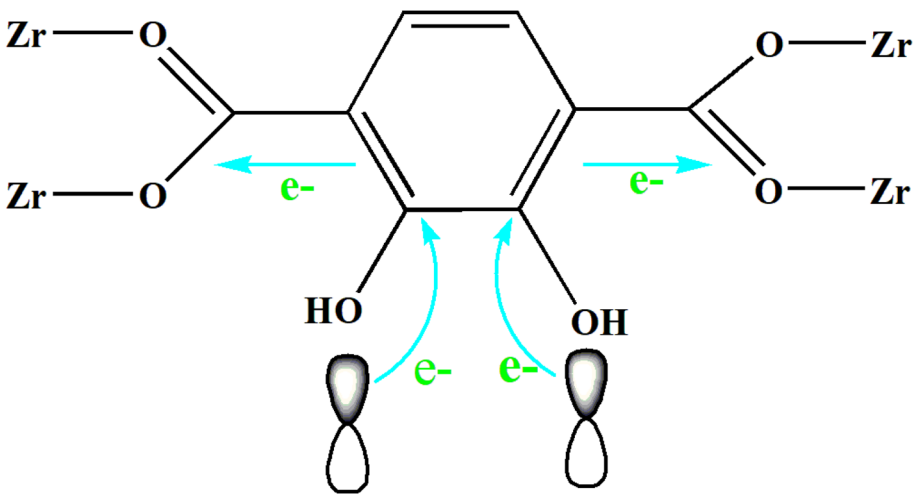

Fig. 10 Mechanism of hydroxy controlling photocatalytic activity.

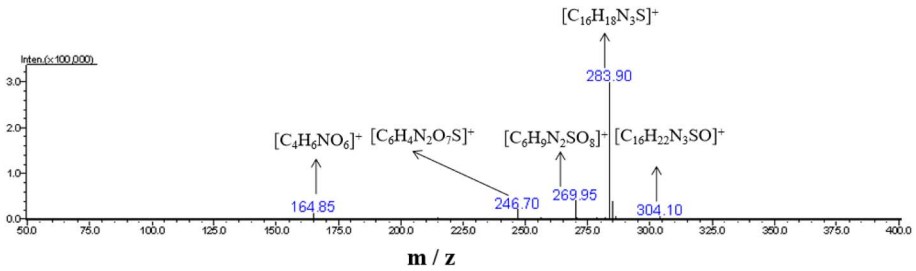

Fig. 12 ESI mass spectra of UIO-66-2OH(2,3) photocatalytic degradation of MB.

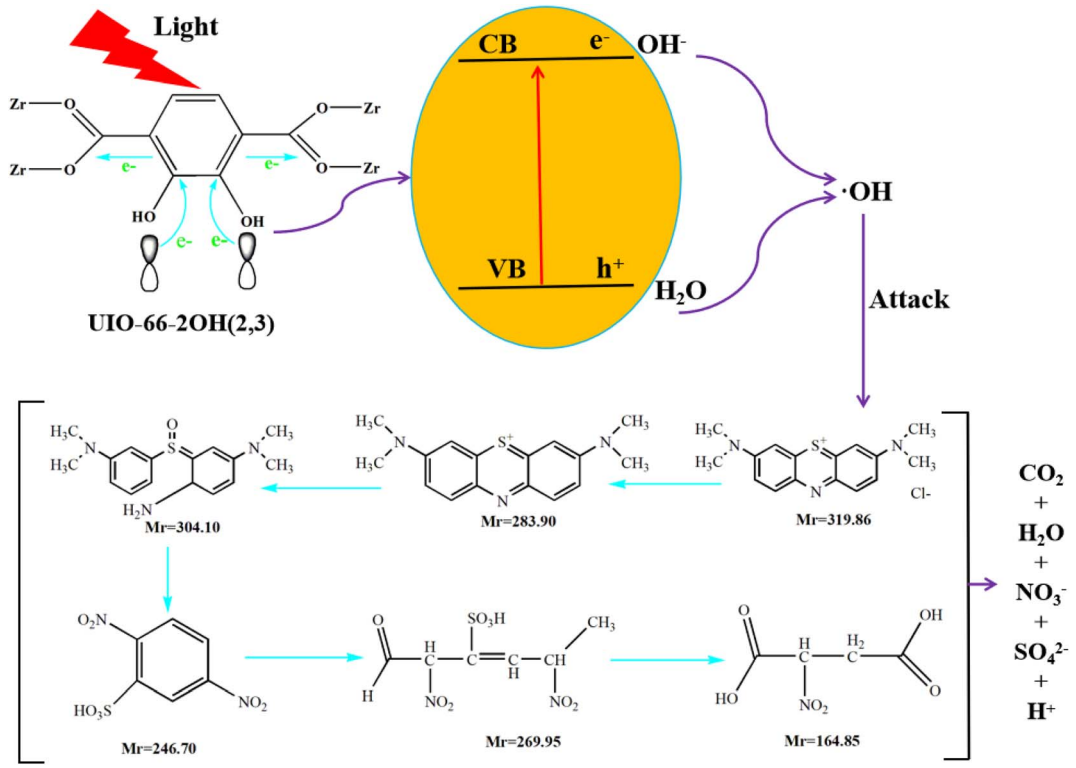

Fig. 13 Mechanism of photocatalytic degradation of MB by UIO-66-2OH(2,3).

degradation of MB showed the characteristic signal peak (1 : 2 : 2 : 1) related to ˙OH.

At pH 1, when UIO-66-2OH(2,3) photocatalytic degrades MB for 20 minutes, high-speed centrifugation is used to remove the photocatalyst, and the solution is collected in the reagent bottle. The products of photocatalytic degradation of MB by UIO-66-2OH(2,3) were analyzed by electrospray ionization mass spectrometry (ESI-MS spectrum). The ESI-MS spectrogram (Fig. 12) shows that there are about five molecular fragment peaks are related to MB decomposition. The MB fragmentation peaks appeared at charge mass ratios (m/z) 164.85, 246.70, 269.95, 283.90 and 304.10. They are $[C_4H_6NO_6]^+$, $[C_6H_4N_2O_7S]^+$, $[C_6H_9N_2SO_8]^+$, $[C_{16}H_{18}N_3S]^+$ and $[C_{16}H_{22}N_3SO]^+$, respectively. The mechanism of photocatalytic degradation MB (Fig. 13) by UIO-66-2OH(2,3) can be clearly judged by analyzing its molecular formula $C_{16}H_{11}N_3SCl$ and ESI-MS characterization results. The MB is a cationic dye, which exists in the form of $[C_{16}H_{18}N_3S]^+$and Cl^- in aqueous solution. The hydroxyl radical (OH˙) generated during the photocatalytic degradation of MB by UIO-66-2OH(2,3) first attacks the S atom and amide bond (-C=N) in $[C_{16}H_{18}N_3S]^+$, thus generating –S=O and $-NH_2$. The result is that the $[C_{16}H_{22}N_3SO]$ is generated. Then, under the attack of ˙OH, the –S=O bond in $[C_{16}H_{22}N_3SO]$ molecule was broken, and $[C_6H_9N_2SO_8]$ was generated. With the continuous attack of ˙OH, the aromatic ring of $[C_6H_9N_2SO_8]$ starts to break and form $[C_6H_4N_2O_7S]$. The –C=C double bond in $[C_6H_4N_2O_7S]$ is oxidized by ˙OH and generates $[C_4H_6NO_6]$. Finally, the C–C single bond of $[C_4H_6NO_6]$ continues to be oxidized by ˙OH and generates CO_2, and H_2O.

4. Conclusion

In summary, the hydroxyl-modified UiO-66 type MOF: UIO-66-2OH(2,3), was successfully synthesized by the method of

ligand exchange by the 2,3-dihydroxyterephthalic acid and UIO-66 as raw materials. It is characterized by Fourier infrared (IR), X-ray powder diffraction (XRD), and X-ray photoelectron spectroscopy (XPS). The results show that its chemical formula is $C_{48}H_{24}Zr_6O_{44}$, which has a similar structure to UIO-66. The photocatalytic degradation performance of UIO-66-2OH(2,3) shows that it has good photocatalytic degradation performance when it is acidic, and under visible light irradiation conditions. At pH = 1, its photocatalytic degradation rate of methylene blue can reach 0.00625 mg min^{-1} L^{-1}. The efficiency of photocatalytic degradation of five cycles can still reach 99.5%. The mechanism of photocatalytic degradation of MB by UIO-66-2OH(2,3) shows that the hydroxyl functional group on the organic ligand regulates its electronegativity and expands its light absorption range. The decomposition of MB is carried out in multiple steps under the oxidation of hydroxyl radical (˙OH).

Author contributions

Shi-Xiong Li designed and conceived the experiments; Guichun Liang, Mulun Yan, and Chengting Wei performed the experiments and analyzed the data; Shaolong Yang used EPR to characterize and analyze the types of free radicals, and modified the grammar of the manuscript; Yan Lu Characterized analyzed the photocatalytic mechanism of photocatalysts; Shi-Xiong Li discussed with all authors and wrote the paper alone; all authors participated in the analysis, interpretation, and review of the results and provided input in the writing process of the paper.

Conflicts of interest

The authors declare no conflict of interest.

Acknowledgements

The authors acknowledge the financial support from Guangxi Natural Science Foundation, China (No. AD19245031, 2019GXNSFBA245063); Basic scientific research ability improvement project of young and middle-aged teachers in Guangxi universities (No. 2023A001); Wuzhou University research foundation for advanced talents (No. WZUQDJJ21081); National College Students Innovation and Entrepreneurship Training Program, China (No. 202211354028).

References

1 S. Li, S. Sun, H. Wu, C. Wei and Y. Hu, Effects of electron-donating groups on the photocatalytic reaction of MOFs, *Catal. Sci. Technol.*, 2018, **8**, 1696–1703.
2 S. Li, Z. Feng, Y. Hu, C. Wei, H. Wu and J. Huang, In-Situ Synthesis and High-Efficiency Photocatalytic Performance of Cu(I)/Cu(II) Inorganic Coordination Polymer Quantum Sheets, *Inorg. Chem.*, 2018, **57**, 13289–13295.
3 X. Liu, Y. Zhang, S. Matsushima, H. Hojo and H. Einaga, Photocatalytic oxidation process for treatment of gas phase benzene using Ti^{3+} self-doped TiO_2 microsphere with sea urchin-like structure, *Chem. Eng. J.*, 2020, **402**, 126220.
4 T. Li, L. Zhao, Y. He, J. Cai, M. Luo and J. Lin, Synthesis of g-C_3N_4/$SmVO_4$ composite photocatalyst with improved visible light photocatalytic activities in RhB degradation, *Appl. Catal., B*, 2013, **129**, 255–263.
5 S. Li, J. Qiang, L. Lu, S. Yang, Y. Chen and B. Liao, In Situ Synthesis Mechanism and Photocatalytic Performance of Cyano-Bridged Cu(I)/Cu(II) Ultrathin Nanosheets, *Front. Chem.*, 2022, **10**, 911238.
6 L. Zeng, F. Zhe, Y. Wang, Q. Zhang, X. Zhao, X. Hu, Y. Wu and Y. He, Preparation of interstitial carbon doped BiOI for enhanced performance in photocatalytic nitrogen fixation and methyl orange degradation, *J. Colloid Interface Sci.*, 2019, **539**, 563–574.
7 Z. Feng, L. Zeng, Q. Zhang, S. Ge, X. Zhao, H. Lin and Y. He, In situ preparation of g-C_3N_4/$Bi_4O_5I_2$ complex and its elevated photoactivity in Methyl Orange degradation under visible light, *J. Environ. Sci.*, 2020, **87**, 149–162.
8 B. Liao and S. Li, Multifunctional Mn (II) Metal-Organic framework for photocatalytic aerobic oxidation and C-H direct trifluoromethylation, *J. Catal.*, 2022, **414**, 294–301.
9 Y. Geng, D. Chen, N. Li, Q. Xu, H. Li, J. He and J. Lu, Z-Scheme 2D/2D α-Fe_2O_3/g-C_3N_4 heterojunction for photocatalytic oxidation of nitric oxide, *Appl. Catal., B*, 2021, **280**, 119409.
10 S. Li, P. Luo, H. Wu, C. Wei, Y. Hu and G. Qiu, Strategies for improving the performance and application of MOFs photocatalysts, *ChemCatChem*, 2019, **11**, 2978–2993.
11 S. Li, Q. Mo, X. Lai, Y. Chen, C. Lin, Y. Lu and B. Liao, Inorganic coordination polymer quantum sheets@ graphene oxide composite photocatalysts: Performance and mechanism, *J. Mater. Res.*, 2019, **34**, 3220–3230.
12 F. Gottschalk, T. Sonderer, R. W. Scholz and B. Nowack, Modeled environmental concentrations of engineered nanomaterials (TiO_2, ZnO, Ag, CNT, fullerenes) for different regions, *Environ. Sci. Technol.*, 2009, **43**, 9216–9222.
13 H. Li, Z. Bian, J. Zhu, Y. Huo, H. Li and Y. Lu, Mesoporous Au/TiO_2 nanocomposites with enhanced photocatalytic activity, *J. Am. Chem. Soc.*, 2007, **129**(15), 4538–4539.
14 J. Huang, S. He, J. L. Goodsell, J. R. Mulcahy, W. Guo, A. Angerhofer and W. D. Wei, Manipulating atomic structures at the Au/TiO_2 interface for O_2 activation, *J. Am. Chem. Soc.*, 2020, **142**, 6456–6460.
15 K. Shahzad, T. Najam, M. S. Bashir, M. A. Nazir, A. ur Rehman, M. A. Bashir and S. S. A. Shah, Fabrication of Periodic Mesoporous Organo Silicate (PMOS) composites of Ag and ZnO: Photo-catalytic degradation of methylene blue and methyl orange, *Inorg. Chem. Commun.*, 2021, **123**, 108357.
16 Y. Zhou, J. He, J. Lu, Y. Liu and Y. Zhou, Enhanced removal of bisphenol A by cyclodextrin in photocatalytic systems: degradation intermediates and toxicity evaluation, *Chin. Chem. Lett.*, 2020, **31**, 2623–2626.
17 Y. Geng, D. Chen, N. Li, Q. Xu, H. Li, J. He and J. Lu, Z-Scheme 2D/2D α-Fe_2O_3/g-C_3N_4 heterojunction for

photocatalytic oxidation of nitric oxide, *Appl. Catal., B*, 2021, **280**, 119409.

18 Y. N. Zhou, R. Li, L. Tao, R. Li, X. Wang and P. Ning, Solvents mediated-synthesis of 3D-BiOX (X= Cl, Br, I) microspheres for photocatalytic removal of gaseous Hg^0 from the zinc smelting flue gas, *Fuel*, 2020, **268**, 117211.

19 O. M. Yaghi and H. Li, Hydrothermal synthesis of a metal-organic framework containing large rectangular channels, *J. Am. Chem. Soc.*, 1995, **117**, 10401–10402.

20 P. Q. Liao, N. Y. Huang, W. X. Zhang, J. P. Zhang and X. M. Chen, Controlling guest conformation for efficient purification of butadiene, *Science*, 2017, **356**, 1193–1196.

21 N. S. Bobbitt, M. L. Mendonca, A. J. Howarth, T. Islamoglu, J. T. Hupp, O. K. Farha and R. Q. Snurr, Metal–organic frameworks for the removal of toxic industrial chemicals and chemical warfare agents, *Chem. Soc. Rev.*, 2017, **46**(11), 3357–3385.

22 J. Wang, C. Rao, L. Lu, S. Zhang, M. Muddassir and J. Liu, Efficient photocatalytic degradation of methyl violet using two new 3D MOFs directed by different carboxylate spacers, *CrystEngComm*, 2021, **23**(3), 741–747.

23 W. Pang, B. Shao, X. Chen, Q. X. Gu, F. J. Yang, S. Li and J. Huang, Enhancing the activity of metal-organic nanosheets for oxygen evolution reaction by substituent effects, *J. Colloid Interface Sci.*, 2022, **608**, 306–312.

24 L. Shi-Xiong, H. Feng-Lan, M. Qiao-Ling and L. Bei-Ling, Synthesis, Characterization and Photocatalytic Mechanism of Hydroxyl Modified MOFs, *Chin. J. Inorg. Chem.*, 2020, **36**, 1401–1412.

25 I. A. Lazaro and R. S. Forgan, Application of zirconium MOFs in drug delivery and biomedicine, *Coord. Chem. Rev.*, 2019, **380**, 230–259.

26 L. Shen, R. Liang, M. Luo, F. Jing and L. Wu, Electronic effects of ligand substitution on metal–organic framework photocatalysts: the case study of UiO-66, *Phys. Chem. Chem. Phys.*, 2015, **17**, 117–121.

27 W. Cao, Y. Yuan, C. Yang, S. Wu and J. Cheng, *In situ* fabrication of g-C_3N_4/MIL-68 (In)-NH_2 heterojunction composites with enhanced visible-light photocatalytic activity for degradation of ibuprofen, *Chem. Eng. J.*, 2020, **391**, 123608.

28 J. Z. Gu, Y. Cai, X. X. Liang, J. Wu, Z. F. Shi and A. M. Kirillov, Bringing 5-(3, 4-dicarboxylphenyl) picolinic acid to crystal engineering research: hydrothermal assembly, structural features, and photocatalytic activity of Mn, Ni, Cu, and Zn coordination polymers, *CrystEngComm*, 2018, **20**, 906–916.

29 Y. Zhao, K. Li and J. Li, Solvothermal synthesis of multifunctional coordination polymers, *Z. Naturforsch., B: J. Chem. Sci.*, 2010, **65**, 976–998.

30 J. Z. Gu, Y. Cai, M. Wen, Z. F. Shi and A. M. Kirillov, A new series of Cd (II) metal–organic architectures driven by soft ether-bridged tricarboxylate spacers: synthesis, structural and topological versatility, and photocatalytic properties, *Dalton Trans.*, 2018, **47**, 14327–14339.

31 L. Shi-Xiong, H. Feng-Lan, B. Yue-Jing, W. Yu-Cai, T. Xue-Li and L. Bei-Ling, Effect of Ions on Photocatalytic Performance of UIO-66-2OH, *Chin. J. Inorg. Chem.*, 2021, **37**(8), 1465–1474.

32 A. Ajmal, I. Majeed, R. N. Malik, H. Idriss and M. A. Nadeem, Principles and mechanisms of photocatalytic dye degradation on TiO_2 based photocatalysts: a comparative overview, *RSC Adv.*, 2014, **4**, 37003–37026.

33 K. Iqbal, A. Iqbal, A. M. Kirillov, B. Wang, W. Liu and Y. Tang, A new Ce-doped MgAl-LDH@ Au nanocatalyst for highly efficient reductive degradation of organic contaminants, *J. Mater. Chem. A*, 2017, **5**, 6716–6724.

34 K. Iqbal, A. Iqbal, A. M. Kirillov, W. Liu and Y. Tang, Hybrid metal–organic-framework/inorganic nanocatalyst toward highly efficient discoloration of organic dyes in aqueous medium, *Inorg. Chem.*, 2018, **57**, 13270–13278.

35 R. Abazari, S. Sanati, A. Morsali and A. M. Kirillov, Instantaneous sonophotocatalytic degradation of tetracycline over NU-1000@ $ZnIn_2S_4$ core–shell nanorods as a robust and eco-friendly catalyst, *Inorg. Chem.*, 2021, **60**, 9660–9672.

36 K. Iqbal, A. Iqbal, A. M. Kirillov, C. Shan, W. Liu and Y. Tang, A new multicomponent CDs/Ag@ Mg–Al–Ce-LDH nanocatalyst for highly efficient degradation of organic water pollutants, *J. Mater. Chem. A*, 2018, **6**, 4515–4524.